Zitierweise:

Supramolecular Chemistry Hot Paper

doi.org/10.1002/anie.202302602

Modulation of Uptake and Reactivity of Nitrogen Dioxide in Metal-Organic Framework Materials

Zi Wang, Alena M. Sheveleva, Daniel Lee, Yinlin Chen, Dinu Iuga, W. Trent Franks, Yujie Ma, Jiangnan Li, Lei Li, Yongqiang Cheng, Luke L. Daemen, Sarah J. Days, Anibal J. Ramirez-Cuesta, Bing Han, Alexander S. Eggeman, Eric J. L. McInnes, Floriana Tuna,* Sihai Yang,* and Martin Schröder**

Abstract: We report the modulation of reactivity of nitrogen dioxide (NO_2) in a charged metal–organic framework (MOF) material, MFM-305-CH_3 in which unbound N-centres are methylated and the cationic charge counter-balanced by Cl^- ions in the pores. Uptake of NO_2 into MFM-305-CH_3 leads to reaction between NO_2 and Cl^- to give nitrosyl chloride (NOCl) and NO_3^- anions. A high dynamic uptake of 6.58 mmol g^{-1} at 298 K is observed for MFM-305-CH_3 as measured using a flow of 500 ppm NO_2 in He. In contrast, the analogous neutral material, MFM-305, shows a much lower uptake of 2.38 mmol g^{-1}. The binding domains and reactivity of adsorbed NO_2 molecules within MFM-305-CH_3 and MFM-305 have been probed using in situ synchrotron X-ray diffraction, inelastic neutron scattering and by electron paramagnetic resonance, high-field solid-state nuclear magnetic resonance and UV/Vis spectroscopies. The design of charged porous sorbents provides a new platform to control the reactivity of corrosive air pollutants.

Introduction

Nitrogen oxide (NO_2) is an important air pollutant that causes serious environmental and health problems.[1–4] It can irritate the respiratory tract, thus increasing the risk of respiratory infections and asthma, particularly for children and people with respiratory problems. Additionally, constant exposure to NO_2 has been linked to an increased risk of heart disease, stroke, and other cardiovascular problems.[5] Although many countries have legislated to restrict the emission of NO_x by vehicles, the concentration of NO_2 in the atmosphere continues to increase.[5] Selective catalytic reductions (SCR) over precious-metal catalysts with toxic reductants (e.g., NH_3) at elevated temperatures are widely applied to convert NO_2 to N_2.[6–8] Alternatively, porous sorbents offer a promising pathways to capture NO_2 under ambient conditions. Conventional porous materials based upon zeolites and activated carbons generally suffer from low uptake and/or severe structural degradations on adsorption of NO_2 owing to its highly reactive and corrosive properties.[9–13]

Metal-organic framework materials show exceptional performance in gas adsorption and storage due to their high porosity and stability.[14–16] Recently, adsorption of NO_2 in MOFs and MOF-based composites has been reported.[17–21] The first example of reversible adsorption of NO_2 in MOFs was achieved by MFM-300(Al), which shows a high uptake

[*] Dr. Z. Wang, Dr. A. M. Sheveleva, Y. Chen, Dr. Y. Ma, Dr. J. Li, Dr. L. Li, Prof. E. J. L. McInnes, Dr. F. Tuna, Prof. S. Yang, Prof. M. Schröder
Department of Chemistry, University of Manchester
Manchester, M13 9PL (UK)
E-mail: eric.mcinnes@manchester.ac.uk
Floriana.tuna@manchester.ac.uk
sihai.yang@manchester.ac.uk
M.Schroder@manchester.ac.uk

Dr. Z. Wang, Dr. A. M. Sheveleva, Prof. E. J. L. McInnes, Dr. F. Tuna
Photon Science Institute, University of Manchester
Manchester, M13 9PL (UK)

Dr. D. Lee
Department of Chemical Engineering and Analytical Science, University of Manchester
Manchester, M13 9PL (UK)

Dr. D. Iuga, Dr. W. T. Franks
Department of Physics, University of Warwick
Coventry, CV4 7AL (UK)

Dr. Y. Cheng, Dr. L. L. Daemen, Dr. A. J. Ramirez-Cuesta
Neutron Scattering Division, Oak Ridge National Laboratory
Oak Ridge, TN 37831 (USA)

Dr. S. J. Days
Diamond Light Source, Harwell Science Campus
Oxfordshire, OX11 0DE (UK)

B. Han, Dr. A. S. Eggeman
Department of Materials, University of Manchester
Manchester, M13 9PL (UK)

of 14.1 mmol g^{-1} at 298 K and 1 bar.[22] UiO-66-NH_2 shows a high adsorption of NO_2 (up to 31.2 mmol g^{-1}) owing to the irreversible chemical reaction with NO_2 to form diazonium species on the aromatic ring of the organic linker, and additionally by reaction with water molecules under humid conditions.[23] However, the molecular details of the reactivity of adsorbed NO_2 molecules within the pore of MOFs have been poorly explored, thus restricting the design of new efficient sorbent materials to mitigate the emission of NO_2.

Here, we report the modulation of reactivity of NO_2 in a pair of closely related MOFs, MFM-305-CH_3 and MFM-305. MFM-305-CH_3, [Al(OH)(L)]Cl, (H_2L)Cl = 3,5-dicarboxy-1-methylpyridinium chloride],[24] has an unusual charged structure incorporating cationic (methylpyridinium) and anionic (Cl^-) components to give a zwitterionic-type framework (Figure 1a). MFM-305-CH_3 has an open framework structure comprised of corner-sharing chains of [AlO_4-$(OH)_2$]$_\infty$ bridged by dicarboxylate ligands. The Al^{III} centres show octahedral coordination defined by four carboxylate oxygen atoms from L^{2-} ligands and two oxygen atoms from two μ_2-hydroxyl groups. MFM-305-CH_3 can undergo post-synthetic modification via heating at 180 °C involving the 1-methylpyridiniumdicarboxylate ligand undergoing in situ demethylation. This is coupled to the loss of Cl^- anion as CH_3Cl to give the pyridyl-based neutral framework in MFM-305 (Figure 1e), which has the same network topology and metal-ligand coordination as MFM-305-CH_3.

We sought to monitor the impact of the differences in these materials on their interaction and reactivity with NO_2. The framework structure in both MFM-305-CH_3 and MFM-305 shows high stability upon adsorption of NO_2. However, adsorption of NO_2 into MFM-305-CH_3 leads to reaction with Cl^- in the pore to give NOCl and NO_3^-, confirmed by in situ infrared (IR), high field solid-state nuclear magnetic resonance (ssNMR) and UV/Vis spectroscopy. The binding domains within the frameworks have been revealed using synchrotron X-ray powder diffraction. A high dynamic uptake of NO_2 of 6.58 mmol g^{-1} at 298 K is observed for MFM-305-CH_3 as measured using a flow of 500 ppm NO_2 in He. NOCl can be extracted with $CHCl_3$ and recovered for use as a reagent for organic synthesis, including N-nitrosation of secondary amines, the structural elucidation of terpenes and the production of aromatic diazonium salts from anilines.[25] Therefore, this work develops a new method for converting NO_2 to useful chemicals, thus converting and utilising a key air pollutant in subsequent chemical processes. MFM-305-CH_3 can be regenerated via ion-exchange and extraction of NO_3^- with Cl^- ions. In contrast, the adsorbed NO_2 molecules in MFM-305 do not react with the framework and an uptake of 2.38 mmol g^{-1} at 298 K is observed. The host–guest binding interactions in both MOFs have been further studied by in situ electron paramagnetic resonance (EPR) spectroscopy and inelastic neutron scattering (INS) coupled with density functional theory (DFT) modelling.

Results and Discussion

Upon introducing NO_2 into MFM-305-CH_3, a yellow-green liquid was observed on cooling the sample to 77 K (Figure 2a). This behaviour is, however, not observed for NO_2-loaded MFM-305. Extracting NO_2-loaded MFM-305-CH_3 with $CHCl_3$ gives a dark orange solution, the UV/Vis spectrum of which shows two bands at 472 and 583 nm

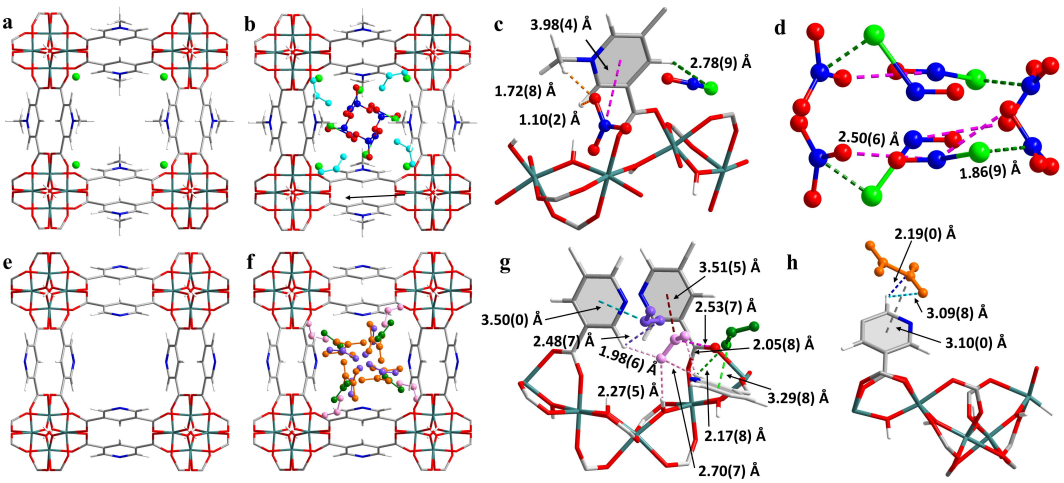

Figure 1. Views of structures of [Al(OH)($C_8H_6NO_4$)Cl] (MFM-305-CH_3), [Al(OH)($C_7H_3NO_4$)] (MFM-305), [Al(OH)($C_8H_6NO_4$)$Cl_{0.78}$·$(NOCl)_{0.22}$·$(NO_3)_{0.22}$·$(NO_2)_{0.5}$] (NO_2-loaded MFM-305-CH_3) and [Al(OH)($C_7H_3NO_4$)·$(NO_2)_{1.7}$·$(NO_2)_{1.0}$·$(NO_2)_{0.45}$·$(N_2O_4)_{0.175}$] (NO_2-loaded MFM-305). All structures were derived from Rietveld refinements of in situ synchrotron X-ray powder diffraction data collected at 298 K (C: grey; N: blue; O: red Al: sea green; H: white; Cl: lime). a) View of MFM-305-CH_3; b) packing of adsorbed NOCl and NO_3^- in MFM-305-CH_3 (viewed down *c* axis) (cyan: NO_2 left after reaction); c) view of binding site of NOCl and NO_3^- in MFM-305-CH_3; d) packing of NOCl-NO_3^- in the pore of MFM-305-CH_3; e) view of MFM-305; f) packing of adsorbed NO_2 and N_2O_4 molecules in MFM-305 (viewed down the *c* axis) (orange: N_2O_4; pink: NO_2 at site I; green: NO_2 at site II; purple: NO_2 at site III); g) view of binding sites of monomer NO_2 in MFM-305; h) view of binding site of N_2O_4 in MFM-305.

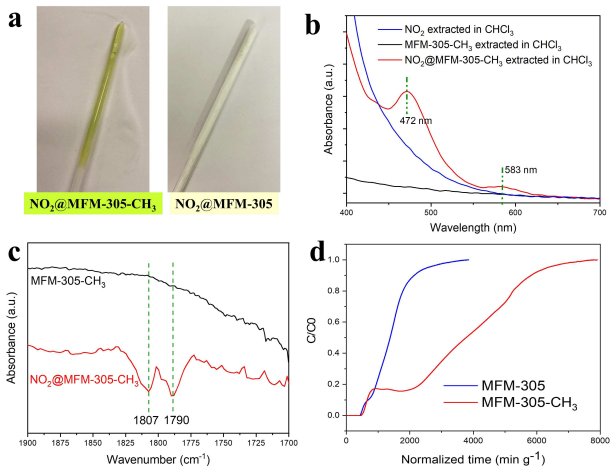

Figure 2. Characterisation of adsorption of NO_2 in MFM-305-CH_3 and MFM-305. a) Photographs of NO_2-loaded MFM-305-CH_3 and MFM-305 at 77 K; b) UV/Vis spectra of $CHCl_3$ solution extracted from NO_2@MFM-305-CH_3 (red), bare MFM-305-CH_3 (black), gas NO_2 (blue); c) in situ DRIFTs of activated (black) and NO_2-loaded MFM-305-CH_3 (red); d) dynamic breakthrough plots of MFM-305-CH_3 and MFM-305 using a gas stream of 500 ppm NO_2 in dry He at 298 K. The normalised concentration represents C/C_0 where C = concentration of NO_2 at outlet, C_0 = concentration of NO_2 at inlet. $C/C_0 = 1$ indicates complete breakthrough.

(Figure 2b) characteristic for NOCl.[25] These bands are absent in the spectra of NO_2 dissolved in $CHCl_3$, and are not observed on extraction of pristine MFM-305-CH_3 with $CHCl_3$, In addition, $CHCl_3$ is unreactive towards N–Cl species, including NOCl, and these observations suggest a chemical reaction of NO_2 taking place within MFM-305-CH_3 involving the Cl^- anions.

In situ diffuse reflectance infrared Fourier transform spectroscopy (DRIFTs) was applied to probe the formation of NOCl. Upon adsorption of NO_2 in activated MFM-305-CH_3, two new peaks appeared at 1790 and 1807 cm^{-1}, assigned as the characteristic ν(N=O) stretching in NOCl interacting with a solid surface, the doublet feature being due to the rotational barrier of the N=O bond upon confinement in the pore (Figure 2c).[26–28] Attempts to identify IR bands for NO_3^- near 1360 and 840 cm^{-1} [27] were hampered due to overlapping peaks from the framework. The reaction between NO_2 and Cl^- has been studied by mixing NO_2 with NaCl as a non-porous material.[27] The reaction at room temperature reaches the equilibrium in 1 h controlled by the limited adsorption of NO_2 onto the external surface of NaCl. In contrast, confined NO_2 molecules within MFM-305-CH_3 react with Cl^- immediately (even at 77 K) due to the presence of strong host–guest interactions. Elemental analysis by inductively coupled plasma atomic emission spectroscopy (ICP-AES) was performed on: (i) the as-synthesised MFM-305-CH_3 [Al(OH)-($C_8H_6NO_4$)Cl·3 H_2O], (ii) re-activated MFM-305-CH_3 after adsorption of NO_2 and removal of NOCl by heating at 100 °C for 10 h under dynamic vacuum [Al(OH)-($C_8H_6NO_4$)NO_3], and (iii) regenerated MFM-305-CH_3 [Al-(OH)($C_8H_6NO_4$)Cl·3 H_2O] by soaking the re-activated material in NaCl-MeOH solution for 3 days (Table S2, Figure S3). The analysis shows that ca. 40 % of the Cl^- anion content was converted to NOCl and removed via the re-activation process, and that ca. 95 % of MFM-305-CH_3 can be regenerated by ion exchange in NaCl solution.

The conversion of NO_2 in MFM-305-CH_3 can also be observed by dynamic breakthrough experiments using a gas stream containing 500 ppm of NO_2 (diluted in He) at 298 K. From 0 to 840 min g^{-1} (quoted as time for breakthrough of NO_2 per gram of porous material, Figure 2d) breakthrough proceeds as normal with NO_2 being expelled from the column. However, from 840 to 2000 min g^{-1}, the detected concentration of NO_2 at the outlet remains unchanged at a normalised concentration of $C/C_0 = 0.2$ consistent with NO_2 molecules introduced to the column being immobilised within the material by reaction with Cl^-. Thus, no additional NO_2 was detected at the outlet during this period up to 2000 min g^{-1}. Once reaction within the pores is complete, the NO_2 can breakthrough as normal as observed after 2000 min g^{-1} (Figure 2d). Thus, MFM-305-CH_3 captures NO_2 by physisorption and then chemisorption via reaction with Cl^- anion leading to an observed increase in its dynamic capacity for NO_2 to 6.58 mmol g^{-1} compared with MFM-305 (2.38 mmol g^{-1}), despite the latter material having a notably larger surface area (256 and 779 $m^2 g^{-1}$, respectively). Thus, the breakthrough plot of dynamic adsorption of NO_2 in MFM-305-CH_3 has a distinct profile and demonstrates the positive impact of reactivity of NO_2 on the adsorption and capture performance of the porous host.[29,30]

To monitor the reaction process, ssNMR spectroscopy was employed at high (23.5 T) and moderate (9.4 T) magnetic fields to investigate the structural changes in MFM-305-CH_3 before and after loading with NO_2. MFM-305-CH_3 has a ^{35}Cl NMR peak at $\delta\{^{35}Cl\} \approx 90$ ppm, which decreases markedly in intensity on adsorption of NO_2 (Figure 3a). To locate the Cl^- ions in the structure of MFM-300-CH_3, a two-dimensional (2D) ^{35}Cl-^{1}H through-space (dipolar) correlation experiment was performed (Figure 3b). Two correlations are observed, with protons at $\delta\{^1H\} \approx 8$ and 12 ppm, which correspond to μ_2-OH and the H1 aromatic proton, respectively. This observation implies the presence hydrogen bonding between these protons and the Cl^- anion (Figure S12), consistent with the Cl^- position as determined by synchrotron X-ray powder diffraction (see below), where Cl^- ions are found to hydrogen-bond to these two sites.[24] ^{1}H NMR assignments in Figure 3b were determined from 2D ^{1}H-^{1}H, ^{1}H-^{13}C and ^{1}H-^{27}Al dipolar correlation spectra (Figures S9a, b and c, respectively). No correlations were be observed in the corresponding 2D ^{35}Cl-^{1}H spectra of NO_2@MFM-305-CH_3 owing to the reduced ^{35}Cl signal (Figure S10).

Upon adsorption of NO_2, the ^{14}N NMR chemical shift of the methylpyridinium nitrogen changes slightly in the 2D ^{14}N-^{1}H dipolar correlation spectrum, and another peak is observed upfield (*cf.* Figure 3c and Figure 3d). Neither peak is observed at the frequency expected for confined NO_3^-,[31] which indicates that the adsorbed species undergoes rapid motion, which averages the guest-host ^{14}N-^{1}H dipolar coupling. Nevertheless, the (at least) two ^{14}N peaks observed

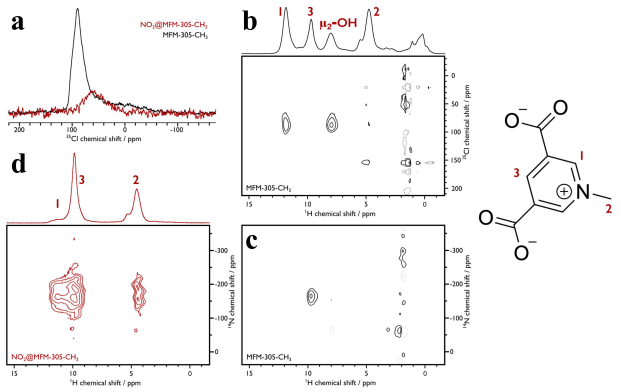

Figure 3. High-field (23.5 T) MAS NMR spectra. a) ^{35}Cl NMR spectra of MFM-305-CH_3 (black) and NO_2@MFM-305-CH_3 (red); b) 2D ^{35}Cl-^{1}H dipolar correlation spectrum of MFM-305-CH_3 with corresponding ^{1}H NMR spectrum (top); c) 2D ^{14}N-^{1}H dipolar correlation spectrum of MFM-305-CH_3; d) 2D ^{14}N-^{1}H dipolar correlation spectrum of NO_2@MFM-305-CH_3 with corresponding ^{1}H NMR spectrum (top). All spectra were recorded at ambient temperature using a MAS frequency of 60 kHz. The 1-methylpyridiniumdicarboxylate ligand is shown (right) with proton environments numbered for the assignments given for the ^{1}H spectra.

for NO_2@MFM-305-CH_3 indicate that the NO_2 induces structural changes at the methylpyridinium N-centre. Moreover, correlations are observed between these two ^{14}N resonances and protons at $\delta\{^1H\} = 4.6$ ppm from the methyl group unlike for pristine MFM-305-CH_3 that does not exhibit ^{14}N-^{1}H correlations with the methyl group. This indicates that the methyl rotation has slowed, likely from hydrogen bonding with NO_3^- (see below), enabling a more efficient dipolar-based transfer of polarisation between methyl ^{1}H and framework ^{14}N centers. Although the NO_3^- is not observed directly by ^{14}N-^{1}H NMR spectroscopy, the presence of hydrogen bonded nitric acid is implied through the differences in ^{1}H spectra between samples and the extremely high-shifted ^{1}H NMR peak that appears (at $\delta\{^1H\} \approx 18$ ppm) upon adsorption of NO_2 (Figure S11b) that can only come from acidic protons involved in hydrogen bonding.[32] The framework structure of the MOF undergoes only a slight modification upon NO_2 adsorption and corresponding loss of Cl^-, with the ligand carbon environments and the octahedral geometry of the aluminium sites undergoing small perturbations, as observed via ^{13}C and ^{27}Al NMR spectroscopy (Figure S9b and Figure S9c, respectively).

A control experiment was designed to monitor how the disproportionation reaction of NO_2 takes place via high-resolution synchrotron X-ray powder diffraction (SPXRD) using a sample of MFM-305-CH_3 loaded with a small amount of NO_2. Rietveld refinement of the SPXRD data gave the formula $[Al(OH)(C_8H_6NO_4)Cl_{0.78}{\cdot}(NOCl)_{0.22}{\cdot}(NO_3)_{0.22}{\cdot}(NO_2)_{0.5}]$. In the refined model (Figure 1b), 22 % of Cl^- anions are converted to NOCl, with formation of the same amount of NO_3^- balancing the charge. The remaining 78 % of Cl^- ions remain at their initial positions (i.e., in the corner of the channel), and the newly-produced guest NOCl is anchored in the pores through the hydrogen bonding to the aromatic proton [$Cl^{NOCl}{\cdots}H3^{aromatic} = 2.78(9)$ Å]. The NO_3^- ions interact with the methyl groups and aromatic protons at a short distance [$O^{NO_3^-}{\cdots}H2^{methyl} = 1.72(8)$ Å and $O^{NO_3^-}{\cdots}H1^{aromatic} = 1.10(2)$ Å] via hydrogen bonding. In addition, a dipole interaction between NO_3^- and the pyridinium group is observed [$O_3N(\delta+)^-{\cdots}py(\delta-) = 3.98(4)$ Å] (Figure 1c). A minor amount of NO_2 (occupancy of 0.5 NO_2/Al) was observed near the corners of the pores upon the equilibrium of the reaction, showing strong hydrogen bonding interaction with the aromatic proton [$O^{NO_2}{\cdots}H1^{aromatic} = 2.15(9)$ Å] and the hydroxyl group [$O^{NO_2}{\cdots}H^{hydroxyl} = 2.88(6)$ Å] (Figure S4). In NO_2-loaded MFM-305 at the same loading, structural analysis gives a model for $[Al(OH)(C_7H_3NO_4){\cdot}(NO_2)_{1.7}{\cdot}(NO_2)_{1.0}{\cdot}(NO_2)_{0.45}{\cdot}(N_2O_4)_{0.175}]$ that shows three different NO_2 binding sites and one N_2O_4 binding site (Figure 1f). The NO_2 molecules at site I (occupancy = 1.7 NO_2/Al) are located in the corner of the pore and exhibit strong hydrogen bonding interaction with the aromatic protons [$O^{NO_2}{\cdots}H1^{aromatic} = 1.98(6)$ Å and 2.05 (8) Å], and with the hydroxyl group [$O^{NO_2}{\cdots}H^{hydroxyl} = 2.27$ (5) Å]. Additional interactions to the carboxylate group [$O_2\underline{N}{\cdots}\underline{O}OC = 2.53(7)$ Å] and the pyridinium ring [$O_2\underline{N}{\cdots}py = 3.51(5)$ Å] are also observed. The NO_2 molecules at site II (occupancy = 1.0 NO_2/Al) are closer to the centre of the pore and interact with the framework via hydrogen bonding [$O^{NO_2}{\cdots}H1^{aromatic} = 2.17(8)$ Å] and are further stabilised by dipole interactions [$O_2\underline{N}{\cdots}py = 3.29(8)$ Å]. NO_2 at site III shows the lowest occupancy (0.45 NO_2/Al) and is located in the middle of the pore [$O^{NO_2}{\cdots}H1^{aromatic} = 2.48(7)$ Å, $O_2\underline{N}{\cdots}py = 3.50(0)$ Å] (Figure 1g). Only a small amount of N_2O_4 was observed (occupancy = 0.35 NO_2/Al), which also shows hydrogen bonding with aromatic protons [$O^{N_2O_4}{\cdots}H1^{aromatic} = 2.19(0)$ Å and 3.09(8) Å] and a dipole interaction [$O_2\underline{N}{\cdots}py = 3.10(0)$ Å] (Figure 1h). The different binding sites also form various monomer-to-monomer, monomer-to-dimer and dimer-to-dimer dipole interactions that stabilise the adsorbed NO_2 molecules in the pore (Figure S6).

In situ INS, coupled with DFT calculations, enabled the direct visualisation of the binding dynamics in NO_2-loaded MFM-305-CH_3 and MFM-305 with a focus on the –CH groups involved in supramolecular contacts (Figure 4). Addition of NO_2 to MFM-305-CH_3 is accompanied by significant changes to peaks at 14 and 26 meV (peaks I and III) consistent with stiffening and deformation of the lattice modes upon binding of NO_2. Another notable change in intensity is observed at 19 meV (peak II), indicating the hindrance of rotation motion of –CH_3 groups upon production of NOCl and NO_3^- species in the pore, consistent with the formation of hydrogen bonds as observed in the structural model. Small changes of intensity were also observed in the high energy region (120–200 meV), which correspond to changes of the aromatic –CH groups (twisting/scissoring/wagging modes) (Figure 4a, S13, S15). The INS spectra of NO_2-loaded MFM-305 gave similar changes in intensities at 17 and 28 meV (peaks I–II) assigned to deformational mode of rings. Moreover, significant changes to peaks at 53, 72, 116 and 123 meV (peaks III–VI) indicate

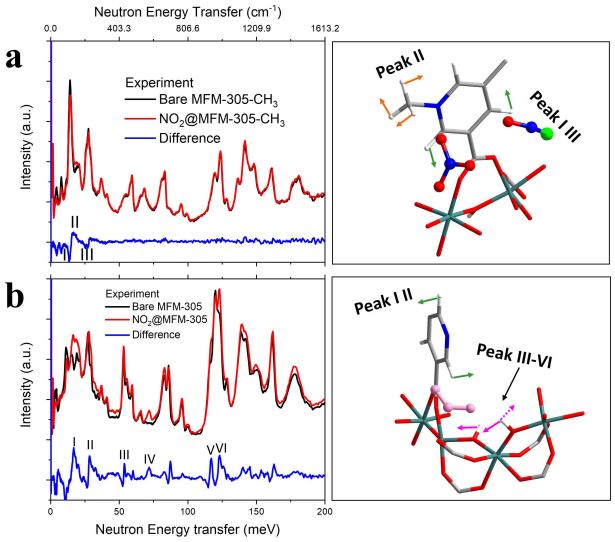

Figure 4. INS spectroscopic data. Comparison of the experimental INS spectra (left) and views of the corresponding structural model (right) for bare and NO_2-loaded a) MFM-305-CH_3 and b) MFM-305.

the bridging hydroxyl is involved in binding to NO_2. Changes in C–H modes also can be observed above 120 meV (Figure 4b, S14, S16). Thus, the results of INS are in good agreement with the in situ crystallographic analyses.

NO_2 is a free radical and thus EPR spectroscopy was used to investigate the host–guest interactions in these two systems under high NO_2 loading. EPR spectra of both NO_2-loaded MFM-305-CH_3 and NO_2-loaded MFM-305 at 10 K show signals from immobilised NO_2 with resolution of the anisotropic electronic g-factor and ^{14}N hyperfine interaction (Figure 5a).[33] These results confirm the presence of immobilised NO_2, and for MFM-305-CH_3, NO_2 is adsorbed into the pores after the disproportionation reaction to form NOCl and NO_3^- has reached equilibrium. Under identical NO_2 loading conditions, the intensity of the NO_2 signal is much lower in MFM-305-CH_3 than in MFM-305 due to the disproportionation reaction in MFM-305-CH_3 (Figure 5b).

The interaction between NO_2 and the framework and other guest molecules is revealed by Davies ENDOR (Electron-Nuclear DOuble Resonance)[34] and ^1H and ^{14}N HYSCORE (Hyperfine Sublevel Correlation) spectroscopies at 10 K. The ENDOR spectra of NO_2-loaded MFM-305-CH_3 were taken at different static magnetic fields (Figure 5b) corresponding to different orientations of the NO_2 molecules. Each spectrum contains features of multiple doublets of protons centred at the proton Larmor frequency. The spectra are dominated by frequencies of ca. 2 MHz which correspond to the nearest e···^1H distances of 3.4 Å in a point dipolar approximation. When MFM-305-CH_3 was synthesised with deuterated methyl groups (MFM-305-CD_3), some weaker ^1H couplings disappear (ca. 1 MHz; corresponding to distances of ca. 4.3 Å), and so these peaks must arise from the methyl protons (Figure S23). The orientation-selective ENDOR measurements confirm that the largest ^1H coupling to the nearest protons are observed along the C_2 (z) axis of the NO_2 molecule, hence the nearest NO_2···^1H distance is approximately in this direction. Calculated ENDOR spectra[35] based on the SPXRD refined structure including the nearest CH_3 and aromatic ^1H positions gave couplings that are too large (Figure S19). The ENDOR spectra were measured at 10 K, and the SPXRD at room temperature, and it appears that on cooling the NO_2 molecules move towards the centre of the pores. Calculated ENDOR spectra based on trial-and-error movement of the NO_2 in the structural model gave good agreement on moving and rotating the NO_2 to the centre of the pore with the nearest protons (H3) along the molecular C_2 axis of NO_2 (Figure 5c, Figure S18), although this model may not be unique. The ENDOR spectra of NO_2-loaded MFM-305 is similar to that of NO_2-loaded MFM-305-CH_3 but with a slightly larger ^1H coupling, indicating the relative position of NO_2 in these two materials are similar but the N···H-(aromatic) distances in MFM-305 are slightly shorter due to the absence of the methyl group (Figure 5d, Figure S21).

^1H HYSCORE spectra for the above materials were collected at identical magnetic field positions and could be simulated with the same models (Figure S28, S29). In addition, weak hyperfine couplings were observed to ^{14}N and ^{27}Al nuclei in the HYSCORE, corresponding to remote nuclei (Figure 5e). In the spectra of NO_2@MFM-305-CH_3, a point-like signal at ca. (3.8, 3.8) MHz represents the interaction between NO_2 molecules and ^{27}Al metal centres from the framework. For NO_2@MFM-305, a similar ^{27}Al signal is observed but, in addition, intense cross-peaks at ca. (2.8, 1.9) and (1.9, 2.8) MHz are observed corresponding to double-quantum signals from a weakly coupled ^{14}N nucleus. These could be reproduced with a point-dipolar ^{14}N hyperfine coupling $|A(^{14}N)| = [1.3, 1.3, -2.0]$ MHz, corresponding to an electron···^{14}N distance of 1.85 Å (Table S7). These ^{14}N signals are not observed in MFM-305-CH_3, and hence cannot be from the pyridyl group but from other guest molecules, consistent with the higher NO_2/N_2O_4 concentration in MFM-305 (Figure 5f).

Conclusion

Our studies reveal a new type of "regenerable reactive adsorption" of NO_2 by modulating the charge in robust MOF materials. MFM-305-CH_3 with a charged pore environment enables the in situ conversion of NO_2 to the usable chemical species NOCl. A full investigation of the reactivity of adsorbed NO_2 molecules, complex and dynamic host–guest binding and detailed structural investigation reveal key molecular details of the conversion of adsorbed NO_2 molecules. The effective control of reactivity of NO_2 achieved by MFM-305-CH_3 provides new insights into the design of efficient protocols for abatement of corrosive air pollutants.

Acknowledgements

We thank the EPSRC (EP/I011870, EP/W014521/1, EP/V035231/1), the Royal Society and the University of Man-

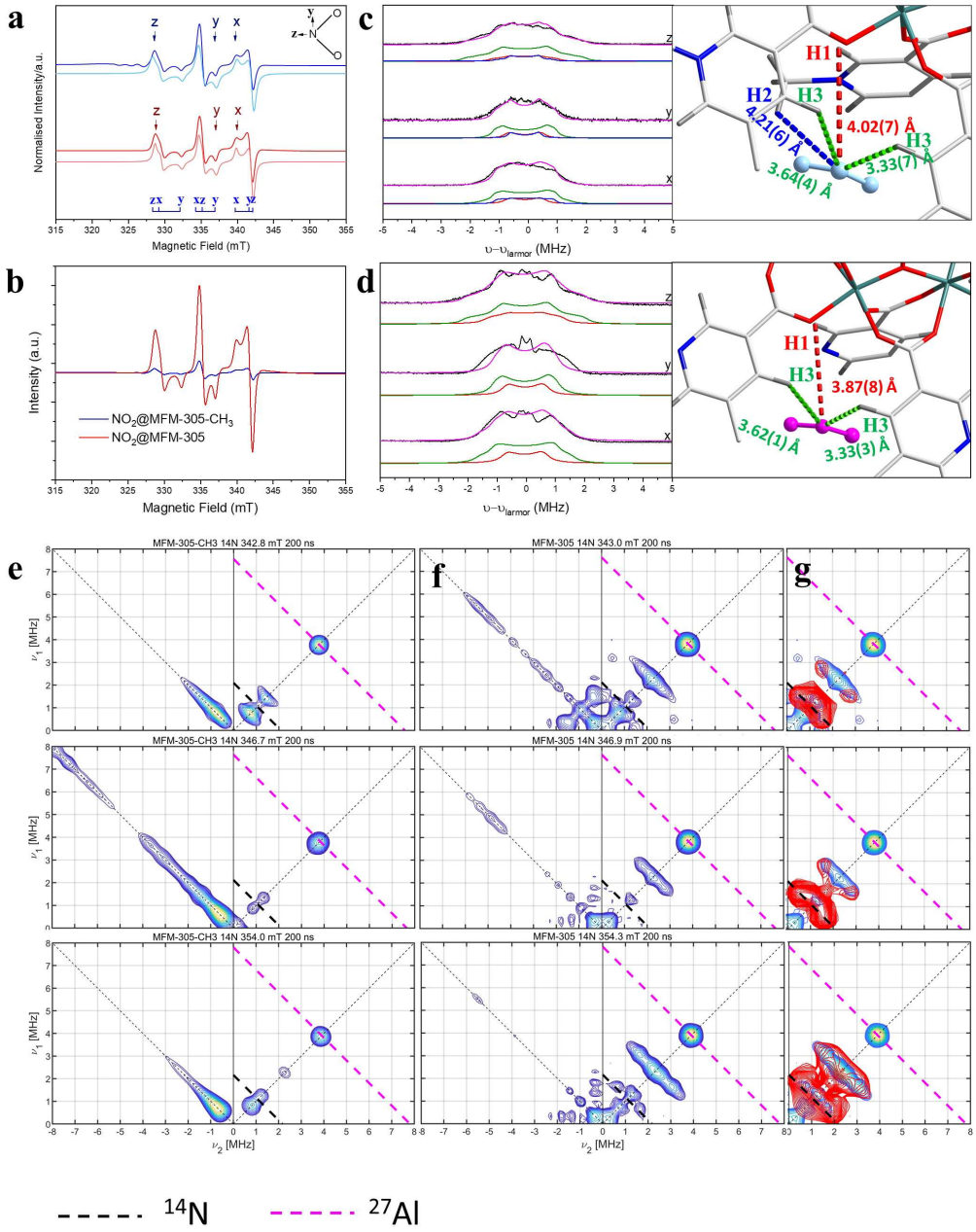

Figure 5. EPR spectroscopic data. a) Continuous-wave X-band (9.72 GHz) EPR spectrum of NO_2@MFM-305-CH_3 at 10 K (blue) and simulation (light blue) with $g_x = 2.0063$, $g_y = 1.9910$ and $g_z = 2.0030$ and ^{14}N nuclear hyperfine interactions (nuclear spin, $I = 1$) of $A_x = 148$, $A_y = 133$ and $A_z = 194$ MHz, where *x*, *y* and *z* define the NO_2 molecular axes (inset). NO_2 has C_{2v} point symmetry with the z axis along the C_2 rotational axis, *y* parallel to the O–O vector and *x* normal to the NO_2 plane; continuous-wave X-band (9.72 GHz) EPR spectrum of NO_2@MFM-305 at 10 K (red) and simulation (light red) with $g_x = 2.006$, $g_y = 1.9913$ and $g_z = 2.0022$ and ^{14}N nuclear hyperfine interactions (nuclear spin, $I = 1$) of $A_x = 144$, $A_y = 133$ and $A_z = 188$ MHz; b) comparison of intensity of EPR signal of NO_2@MFM-305-CH_3 and NO_2@MFM-305 under identical conditions; X-band Davies ENDOR spectrum of c) NO_2@ MFM-305-CH_3 and d) NO_2@MFM-305 (black) at 5 K and the static magnetic fields indicated, shown by the arrows in (a), selecting the NO_2 *x*, *y* and *z* axes (bottom to top), respectively. ENDOR gives pairs of transitions separated by the effective hyperfine coupling for the orientations selected, centred on the Larmor frequency of the nucleus being probed (14.9 MHz for ^{1}H at 350 mT), and its simulated spectra (magenta for sum; red, green and blue for different protons); view of binding site of c) NO_2 in MFM-305-CH_3 and d) NO_2 in MFM-305 after movement and rotation attached; X-band (9.7368 GHz) ^{14}N HYSCORE spectra of e) NO_2@MFM-305-CH_3 measured at static fields 342.8, 346.7 and 354.0 mT, and of f) NO_2@MFM-305 measured at static fields 343.0, 346.9 and 354.3 mT; g) simulated spectra (red) with parameters in Table S7. The anti-diagonal dashed lines cross the diagonal at the Larmor frequencies for ^{14}N and ^{27}Al (black: ^{14}N; magenta: ^{27}Al).

chester for funding, and the EPSRC for funding of the EPSRC National EPR Facility at Manchester. This project has received funding from the European Research Council (ERC) under the European Union's Horizon 2020 research and innovation program (grant agreement No 742401, *NANOCHEM*). The UK High-Field Solid-State NMR

Facility used in this research was funded by EPSRC and BBSRC (EP/T015063/1), as well as, for the 1 GHz instrument, EP/R029946/1. We are grateful to Diamond Light Source and Oak Ridge National Laboratory (ORNL) for access to Beamlines I11 and VISION (a DOE Office of Science User Facility), respectively. The computing resources were made available through the VirtuES and the ICE-MAN projects, funded by Laboratory Directed Research and Development program and Compute and Data Environment for Science (CADES) at ORNL. A.M.S. was supported by the Royal Society Newton International Fellowship.

Conflict of Interest

The authors declare no conflict of interest.

Data Availability Statement

The data that support the findings of this study are available in the Supporting Information of this article.

Keywords: Conversion · Metal–Organic Framework · Nitrogen Dioxide · Reactivity Modulation · Spectroscopy

[1] J. Lelieveld, T. M. Butler, J. N. Crowley, T. J. Dillon, H. Fischer, L. Ganzeveld, H. Harder, M. G. Lawrence, M. Martinez, D. Taraborrelli, J. Williams, *Nature* **2008**, *452*, 737–740.
[2] P. M. Edwards, S. S. Brown, J. M. Roberts, R. Ahmadov, R. M. Banta, J. A. deGouw, W. P. Dubé, R. A. Field, J. H. Flynn, J. B. Gilman, M. Graus, D. Helmig, A. Koss, A. O. Langford, B. L. Lefer, B. M. Lerner, R. Li, S.-M. Li, S. A. McKeen, S. M. Murphy, D. D. Parrish, C. J. Senff, J. Soltis, J. Stutz, C. Sweeney, C. R. Thompson, M. K. Trainer, C. Tsai, P. R. Veres, R. A. Washenfelder, C. Warneke, R. J. Wild, C. J. Young, B. Yuan, R. Zamora, *Nature* **2014**, *514*, 351–354.
[3] M. G. Ghozikali, M. Mosaferi, G. H. Safari, J. Jaafari, *Environ. Sci. Pollut. Res. Int.* **2015**, *22*, 2817–2823.
[4] E. Dons, M. Laeremans, E. Anaya-Boig, I. Avila-Palencia, C. Brand, A. de Nazelle, M. Gaupp-Berghausen, T. Götschi, M. Nieuwenhuijsen, J. P. Orjuela, E. Raser, A. Standaert, L. Int Panis, *Air Qual. Atmosphere Health* **2018**, *11*, 591–599.
[5] "Nitrogen dioxide (NO_2) pollution, 2019. United States Environmental Protection Agency Website" can be found under https://www.epa.gov/NO_2-pollution.
[6] J.-H. Park, J.-W. Ahn, K.-H. Kim, Y.-S. Son, *Chem. Eng. J.* **2019**, *355*, 351–366.
[7] B. Guan, R. Zhan, H. Lin, Z. Huang, *Appl. Therm. Eng.* **2014**, *66*, 395–414.
[8] M. Iwasaki, H. Shinjoh, *Appl. Catal. A* **2010**, *390*, 71–77.
[9] J. M. Goupil, J.-F. Hemidy, D. Cornet, *Zeolites* **1982**, *2*, 47–50.
[10] M. Belhachemi, M. Jeguirim, L. Limousy, F. Addoun, *Chem. Eng. J.* **2014**, *253*, 121–129.
[11] M. Florent, M. Tocci, T. J. Bandosz, *Carbon* **2013**, *63*, 283–293.
[12] N. Shirahama, S. H. Moon, K.-H. Choi, T. Enjoji, S. Kawano, Y. Korai, M. Tanoura, I. Mochida, *Carbon* **2002**, *40*, 2605–2611.
[13] X. Zhou, Z. Su, H. Chen, X. Xiao, Y. Qin, L. Yang, Z. Yan, W. Sun, *Mol. Phys.* **2018**, *116*, 2095–2107.
[14] Y. Li, R. T. Yang, *Langmuir* **2007**, *23*, 12937–12944.
[15] J. R. Li, R. J. Kuppler, H.-C. Zhou, *Chem. Soc. Rev.* **2009**, *38*, 1477–1504.
[16] T. Ghanbari, F. Abnisa, W. M. A. Wan Daud, *Sci. Total Environ.* **2020**, *707*, 135090.
[17] T. Islamoglu, Z. Chen, M. C. Wasson, C. T. Buru, K. O. Kirlikovali, U. Afrin, M. R. Mian, O. K. Farha, *Chem. Rev.* **2020**, *120*, 8130–8160.
[18] A. M. Ebrahim, B. Levasseur, T. J. Bandosz, *Langmuir* **2013**, *29*, 168–174.
[19] A. M. Ebrahim, T. J. Bandosz, *ACS Appl. Mater. Interfaces* **2013**, *5*, 10565–10573.
[20] B. Levasseur, C. Petit, T. J. Bandosz, *ACS Appl. Mater. Interfaces* **2010**, *2*, 3606–3613.
[21] C. Petit, B. Levasseur, B. Mendoza, T. J. Bandosz, *Microporous Mesoporous Mater.* **2012**, *154*, 107–112.
[22] X. Han, H. G. W. Godfrey, L. Briggs, A. J. Davies, Y. Cheng, L. L. Daemen, A. M. Sheveleva, F. Tuna, E. J. L. McInnes, J. Sun, C. Drathen, M. W. George, A. J. Ramirez-Cuesta, K. M. Thomas, S. Yang, M. Schröder, *Nat. Mater.* **2018**, *17*, 691–696.
[23] G. W. Peterson, J. J. Mahle, J. B. DeCoste, W. O. Gordon, J. A. Rossin, *Angew. Chem. Int. Ed.* **2016**, *55*, 6235–6238.
[24] L. Li, I. da Silva, D. I. Kolokolov, X. Han, J. Li, G. Smith, Y. Cheng, L. L. Daemen, C. G. Morris, H. G. W. Godfrey, N. M. Jacques, X. Zhang, P. Manuel, M. D. Frogley, C. A. Murray, A. J. Ramirez-Cuesta, G. Cinque, C. C. Tang, A. G. Stepanov, S. Yang, M. Schröder, *Chem. Sci.* **2019**, *10*, 1472–1482.
[25] R. Lebl, D. Cantillo, C. O. Kappe, *React. Chem. Eng.* **2019**, *4*, 738–746.
[26] S. J. Peters, G. E. Ewing, *J. Phys. Chem.* **1996**, *100*, 14093–14102.
[27] B. J. Finlayson-Pitts, *Nature* **1983**, *306*, 676–677.
[28] W. H. Schroeder, P. Urone, *Environ. Sci. Technol.* **1974**, *8*, 756–758.
[29] A. Hanif, M. Sun, T. Wang, S. Shang, D. C. W. Tsang, J. Shang, *J. Cleaner Prod.* **2021**, *313*, 127956.
[30] S. Shang, C. Yang, Y. Tian, Z. Tao, A. Hanif, M. Sun, H. H. S. Wong, C. Wang, J. Shang, *ACS ES&T Eng.* **2021**, *1*, 375–384.
[31] X. Hou, R. J. Kirkpatrick, P. Yu, D. Moore, Y. Kim, *Am. Mineral.* **2000**, *85*, 173–180.
[32] Y. Ma, X. Han, S. Xu, Z. Wang, W. Li, I. da Silva, S. Chansai, D. Lee, Y. Zou, P. Manual, A. M. Sheveleva, F. Tuna, E. J. L. McInnes, Y. Cheng, S. Rudić, A. J. Ramirez-Cuesta, S. J. Haigh, C. Hardacre, M. Schröder, S. Yang, *J. Am. Chem. Soc.* **2021**, *143*, 10977–10985.
[33] M. Shiotani, J. H. Freed, *J. Phys. Chem.* **1981**, *85*, 3873–3883.
[34] E. R. Davies, *Phys. Lett. A* **1974**, *47*, 1–2.
[35] S. Stoll, A. Schweiger, *J. Magn. Reson.* **2006**, *178*, 42–55.

Manuscript received: February 20, 2023
Accepted manuscript online: April 7, 2023
Version of record online: April 7, 2023

Forschungsartikel

Supramolecular Chemistry

Z. Wang, A. M. Sheveleva, D. Lee, Y. Chen, D. Iuga, W. T. Franks, Y. Ma, J. Li, L. Li, Y. Cheng, L. L. Daemen, S. J. Days, A. J. Ramirez-Cuesta, B. Han, A. S. Eggeman, E. J. L. McInnes,* F. Tuna,* S. Yang,* M. Schröder* **e202302602**

Modulation of Uptake and Reactivity of Nitrogen Dioxide in Metal-Organic Framework Materials

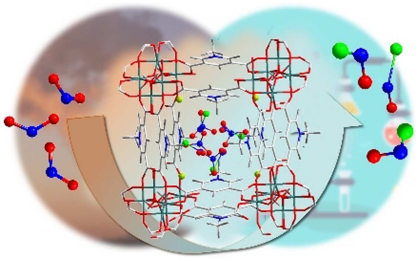

The reactivity of NO_2 is modulated in a charged metal–organic framework, MFM-305-CH_3, which leads to reaction between NO_2 and framework Cl^- to give nitrosyl chloride (NOCl) and NO_3^- anions. A higher NO_2 dynamic uptake (6.58 mmol g^{-1}) is achieved, compared with the analogous neutral material, MFM-305 (2.38 mmol g^{-1}).